


FULL PAPER

An atmospheric pressure non-self-sustained glow discharge in between metal/metal and metal/liquid electrodes

Ivana Sremački¹ | Mikhail Gromov^{1,2}  | Christophe Leys¹ | Rino Morent¹ | Rony Snyders^{2,3} | Anton Nikiforov¹

¹Department of Applied Physics, Ghent University, Gent, Belgium

²Chimie des Interactions Plasma-Surface (ChIPS), CIRMAP, Mons University, Mons, Belgium

³Materia Nova Research Centre, Parc Initialis, Mons, Belgium

Correspondence

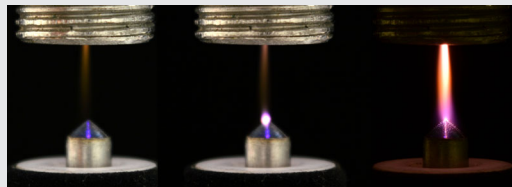
Anton Nikiforov, Department of Applied Physics, Ghent University, Sint-Pietersnieuwstraat 41, 9000 Gent, Belgium.
Email: Anton.Nikiforov@UGent.be

Funding information

FWO/ARRS Agencies, Grant/Award Numbers: G084917N, N3-0056; NITROPLASM EOS Project, Grant/Award Number: ID: 30505023

Abstract

Non-thermal plasmas operating at high pressure attract increasing attention for a variety of applications as an alternative to conventional chemical processes. In this study, an atmospheric pressure direct current non-self-sustained discharge in nitrogen is investigated as a source of non-thermal plasma capable of operating in a glow regime. The discharge is sustained between an internal source of ionization and a metal or liquid electrode and studied by electrical diagnostics as well as by spectroscopy methods. The work is focused on the determination of the discharge properties including vibrational and gas temperature. The effect of the liquid electrode on the discharge properties is studied and analyzed. The mechanisms of the discharge sustaining and pathways of nitrogen state excitation are discussed.



KEYWORDS

liquid anode, nitrogen, non-self-sustained glow discharge, optical emission spectroscopy, vibrational excitation

1 | INTRODUCTION

Non-equilibrium plasmas at atmospheric pressure have got a lot of attention from the scientific community and have already found a place in a variety of applications ranging from gas purification to film deposition and plasma medicine.^[1–3] Among a variety of applications, the N₂ fixation to valuable products by electrical discharge has very large potential. Almost a century ago, thermal arc furnaces were successfully developed and implemented to

convert air into nitrogen oxides. Unfortunately, the low NO_x yield and low energy efficiency in regard to the Haber–Bosch (H–B) process, banned the process from the industry.^[4,5]

Nowadays, there is a hope that alternative methods for N₂ conversion based on biological, metal-complex approaches, or use of non-thermal plasmas (NTP) can replace the H–B process.^[6] The NTP approach is based on vibrational–vibrational excitation and electron-impact processes in the N₂ mixture with O₂, H₂O, or CH₄ gas at high pressure. Thereby, a high N₂ conversion to either NO_x or NH₃ or HNO₃ at low reaction temperature and low energy consumption can be achieved.^[7] The theoretical limit of energy consumption of N₂ conversion via

Ivana Sremački and Mikhail Gromov contributed equally to this study.

NTP is more than 2.5 times lower than the energy consumption of the H–B process.^[6]

One of the obstacles in the operation of atmospheric pressure discharges in nitrogen rich mixtures is the development of instabilities.^[8–10] A transition from a glow to a spark or an arc discharge is often observed due to an imbalance between the ionization and the recombination processes. The imbalance can take place through local heating and formation of the gas temperature gradients as a result of fluctuations in the electron density, stepwise ionization, electron loss processes that strongly depend on electron temperature T_e .^[11]

The formation of sparks and discharge transition to arc can be suppressed by limiting the discharge current. This can be achieved by adding passive elements in series with discharge. In direct current (DC) plasmas, a resistive ballast with relatively high resistance of 10s–100s of k Ω can be implemented. However, the using of passive components will not necessarily prevent the appearing of constricted current channels and their usage can also reduce the total energy efficiency of a process due to large energy dissipation on capacitive elements. This problem can be solved by using a distributed ballast, that is, a resistive electrode made of a resistive ceramic or using a liquid with limited conductivity as an electrode. The well-known heating instabilities^[12] can be often controlled by the use of high gas flow through the plasma bulk. Discharge stabilization by high gas flow not only excludes the local thermal instabilities but also allows controlling the residence time of the plasma species by regulating gas velocity. An alternative approach to eliminate the discharge constriction is to reduce the discharge duration below the characteristic time of instabilities' development.

One of the very effective methods to prevent instabilities and create large volume atmospheric pressure plasmas is the operation of the discharge in the non-self-sustained regime. These plasmas have an internal ionization source which provides electrons and ions for further ionization and excitation. The dominance of ionization processes over recombination in non-self-sustained discharges results in high discharge stability as the ionization is made by an additional source.^[1]

In the case of an atmospheric pressure glow discharge, the most common instability is glow-to-arc transition (GAT). At atmospheric pressure, the shrinkage of the cathode layer leads to high current density near the cathode, and consequently, to the arc transition. The GAT instability can be avoided by adding an additional internal source of electrons that will suppress the importance of the cathode area of the glow discharge. The example of the NS-GD realization is a micro hollow cathode sustained glow discharge (MCSGD). The conception of MCSGD was proposed and studied in detail by Stark and Schoenbach.^[13–16] The discharge consists

of a three-electrode DC plasma in which a micro hollow cathode discharge (MHCD) in between two electrodes is used as a virtual plasma cathode to eliminate the cathode region. A detailed description of MHCD operated in different gases can be found in References^[17–19]. The third electrode in MCSGD is used as an anode and located in front of the ground flat electrode of the MHCD at a distance up to 10 mm. At a considerable high value of the electrical field of the MHCD, the flow of high-energy electrons is injected in the main gap of the MCSGD and the normal glow discharge is formed. Therefore, the non-self-sustained discharge stability is defined by the stability of the operation of the internal source, micro hollow discharge. Previously,^[13] it was shown that MCSGD discharge can be generated in a stable regime, with negligible current fluctuations and low sputtering of the electrodes resulting in a long lifetime.

In the present work, atmospheric pressure NS-GD in nitrogen flow has been generated by using a DC-driven plasma jet as an internal source of ionization. The discharge was generated between a plasma jet that plays the role of the virtual cathode and an additional anode. The advantage of such a configuration is related to the high stability of the plasma jet operation and the almost negligible effect of the erosion of the electrodes, which is one of the drawbacks of the MHSGD. Glow discharge has been successfully generated above the metal electrode as well as above a solution of sodium dihydrophosphate. The discharge was investigated in terms of its electrical properties, space-resolved rotational and vibrational temperature, and translational (gas) temperature. Special attention was paid to excitation kinetics of nitrogen states and electrical field determination.

2 | EXPERIMENTAL SETUP

The non-self-sustained DC glow discharge (NS-GD) generated in pure nitrogen under ambient conditions was generated between metal and metal/liquid electrodes. It has to be emphasized that the DC plasma jet was used as an internal source of ionization to replace the cathode spot and so to stabilize the discharge. Accordingly, removing or switching off the plasma jet leads to the extinguishing of the whole discharge. NS-GD in the metal and liquid anodes was investigated by means of electrical and temperature characterization. The kinetics of N₂ molecule excitation in both cases was analyzed.

2.1 | Non-self-sustained discharge

The schematic of the discharge is presented in Figure 1 with a schematic drawing of the typical discharge

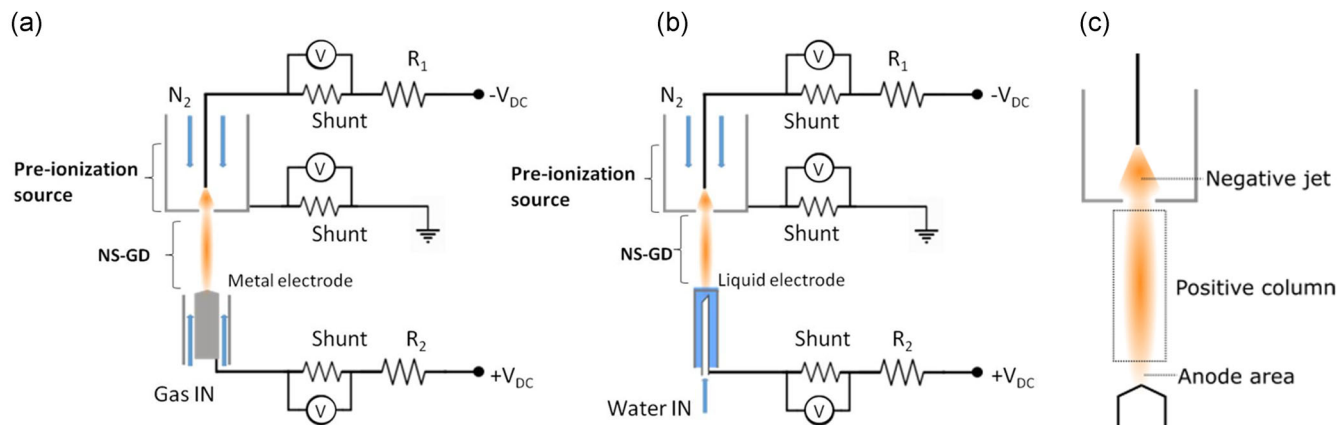


FIGURE 1 Experimental setups and electrode design. (a) NS-GD with the metal additional electrode. (b) NS-GD with the liquid additional electrode. (c) Schematic representation of the NS-GD regions. The plasma diagnostics system is not shown. NS-GD, non-self-sustained DC glow discharge

structure (Figure 1c). The internal source of ionization was ignited between the negatively powered pin electrode ($d = 1$ mm) by means of a DC high-voltage power supply (Fluke 415 A high-voltage DC power supply) through a ballast resistor $R_1 = 100$ k Ω and grounded nozzle ($d_{\text{hole}} = 2$ mm). The jet with a long afterglow of about 4 mm was formed in N_2 flow and used as the source of internal ionization. As shown in the experimental scheme in Figure 1, two different additional electrode designs were applied to generate NS-GD:

1. Negative jet—solid electrode;
2. Negative jet—liquid electrode.

Applying a positive high voltage (Fluke 408B high-voltage DC power supply) to an additional electrode (solid and liquid) through $R_2 = 50$ k Ω ballast, a glow discharge of length 6 mm and diameter of about 2 mm is formed. In the case of solid electrodes, the N_2 flow rate was set at 2 SLM between the negative pin and ground electrode (top) and 1.5 SLM at the bottom compartment. Both cathode pin and solid anode were made of tungsten to suppress sputtering and thermal erosion of the electrodes. The flow of 10 ml/min of sodium dihydrogen phosphate (NaH_2PO_4) solution in water with the conductivity of $\sigma = 350$ $\mu S/cm$ controlled by the syringe pump was used in the case of the liquid electrode. Indicated liquid flow through the anode was chosen to minimize the evaporation effect and so to decrease the presence of water vapor in the discharge and ensure its stable operation without arcing or extinguishing of the plasma column. The electrical current was measured as the current through two different shunt resistors with 462 Ω resistance, as shown in the experimental scheme. An applied voltage across the NS-GD and the internal source of ionization were measured by DC high-voltage

probes (HP 34111A high-voltage probe, Fluke 80K-40 high-voltage probe). The breakdown voltage required for the generation of the jet was fixed through all experiments at 3.2 kV. During all experiments, the current through the jet was maintained at 7 mA that corresponds to the applied voltage of 1 kV.

2.2 | Electrical field measurement

To estimate the electrical field, the voltage of the positive column (Figure 1c) in glow discharge was measured as a function of the interelectrode distance. The current for different gaps was maintained constant at 17 mA, whereas the voltage was measured with high-voltage probes as a potential difference between the anode and the ground electrode. The gap between electrodes was varied in the range of 6–1 mm and from 6 to 3 mm for the solid and liquid electrode, respectively. The intersection of applied voltage with the ordinate axis gives the voltage drop on the bottom electrode whereas the slope of the plot is used to estimate the electrical field.

2.3 | Plasma temperature diagnostics

The efficiency of conventional processes of nitrogen fixation to NO_x species strongly correlates with gas-phase temperature due to the endothermic nature of the reactions,^[20] meaning high energy costs. Owing to their high reactivity at relatively low gas temperature T_{gas} , non-equilibrium plasmas are providing an alternative pathway for gas conversion because of the possibility to decrease the reaction energy barrier through increasing only electron T_e and vibrational temperature T_{vib} keeping the translation temperature relatively low. Accordingly,

plasma temperature characterization techniques, namely optical emission spectroscopy (OES) and Rayleigh scattering spectroscopy were used here to determinate rotational, vibrational, and translational N_2 temperatures.

2.3.1 | Optical emission spectroscopy

Both rotational (T_{rot}) and vibrational (T_{vib}) temperature determination methods assume Boltzmann distribution of rotational/vibrational states, thus OES temperature measurements were based on relative intensity measurements of spectral lines of a second positive system (SPS) of nitrogen N_2 $C^3\Pi_u \rightarrow B^3\Pi_g$.^[21] The band N_2 $C^3\Pi_u \rightarrow B^3\Pi_g$ was analyzed for the determination of N_2 rotational temperature. Intensities of vibrational sequence $\Delta\nu = 2$, 0–2 (head maximum 380.4 nm), 1–3 (375.4 nm), 2–4 (370.9), and 3–5 (367.1 nm) were recorded to obtain temperature T_{vib} . MassiveOES software^[22,23] was used to fit N_2 $C^3\Pi_u \rightarrow B^3\Pi_g$ experimental and theoretical spectra, providing T_{rot} and T_{vib} as a result of the fitting process. The discharge emission was collected with ceramics ferrule fiber ($d = 200 \mu m$) allowing spatially resolved measurement in three different positions with a 2-mm diameter of the collecting region (cathode area, positive column, and anode area) as shown in Figure 3 (see Section 3.1). An Avantes spectrometer with a resolution about $R = 0.05$ nm was used to partially resolve the rotational structure of the N_2 $C^3\Pi_u \rightarrow B^3\Pi_g$ bands. The calibration of the spectrometer was carried out with a Tungsten halogen lamp (250–2,400 nm). The rotational and vibrational temperatures were determined with an uncertainty lower than 10%. The full range spectrum of NS-GD was recorded with an Ocean Optics S2000 spectrometer with a resolution of 1.7 nm calibrated with a tungsten halogen lamp.

2.3.2 | Rayleigh scattering spectroscopy

Rayleigh scattering spectroscopy was carried out to estimate gas temperature.^[24,25] The intensity of elastically scattered laser light on heavy species present in plasma is directly proportional to the density of species n_g^i that can be correlated to their temperature (T_g):

$$I \sim \sum_i \sigma^i \frac{p^i}{k_B T_g}, \quad (1)$$

where σ^i , p^i , k_B are the Rayleigh scattering cross-section of species, the partial pressure of scatters and Boltzmann constant. Gas temperature (T_g) in plasma was calculated as a ratio of scattered laser light intensity (I_{ref}) corresponding

to the known reference temperature (T_{ref}) and scattered intensity when it passes through a plasma (I_p):

$$T_g = \frac{I_{ref}}{I_p} T_{ref}. \quad (2)$$

Pulsed Nd:YAG laser (Litron nano-S) was used at a wavelength of 532 nm for Rayleigh scattering spectroscopy. The repetition rate was 10 Hz, the energy of the pulse was 12 ± 1 mJ, which was measured with an OphirPhotonics power meter. The laser beam has a Gaussian shape with a diameter of 0.5 mm. A fast imaging gated Hamamatsu digital camera with a 532-nm filter with FWHM of 10 nm was used to record a scattered signal. The synchronization between the laser pulse and the camera gate unit was achieved using a Stanford Research DG535 delay generator. The experimental setup for Rayleigh scattering spectroscopy is shown in Figure 2. A quartz prism was used to deflect the direction of beam propagation to 90°. After deflection, the beam was focused with a lens $f = 500$ mm resulting in a beam diameter of 0.5 mm in the region of interest. Gas temperature was measured in the middle of the plasma (position 2 in Figure 3) to suppress reflections of the laser beam from the solid anode, whereas for the liquid electrode it was closer to position 1 due to the formation of water microdroplets and stronger beam reflection. Rayleigh scattering spectroscopy was carried out in ambient conditions, 10 laser shots were integrated and 10 images were analyzed for each condition, and images not affected by Mie scattering on dust particles were considered valid for temperature determination. Gas temperature was measured with an error of $\pm 10\%$ appearing mainly due to a fluctuation of the laser energy.

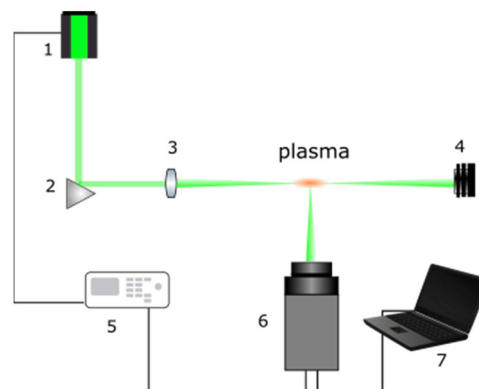


FIGURE 2 Experimental schematic of the setup for the Rayleigh scattering spectroscopy. 1: Nd:YAG laser at 532 nm, 2: Prism, 3: Telescope, 4: Beam dump, 5: Delay generator, 6: Camera, and 7: PC

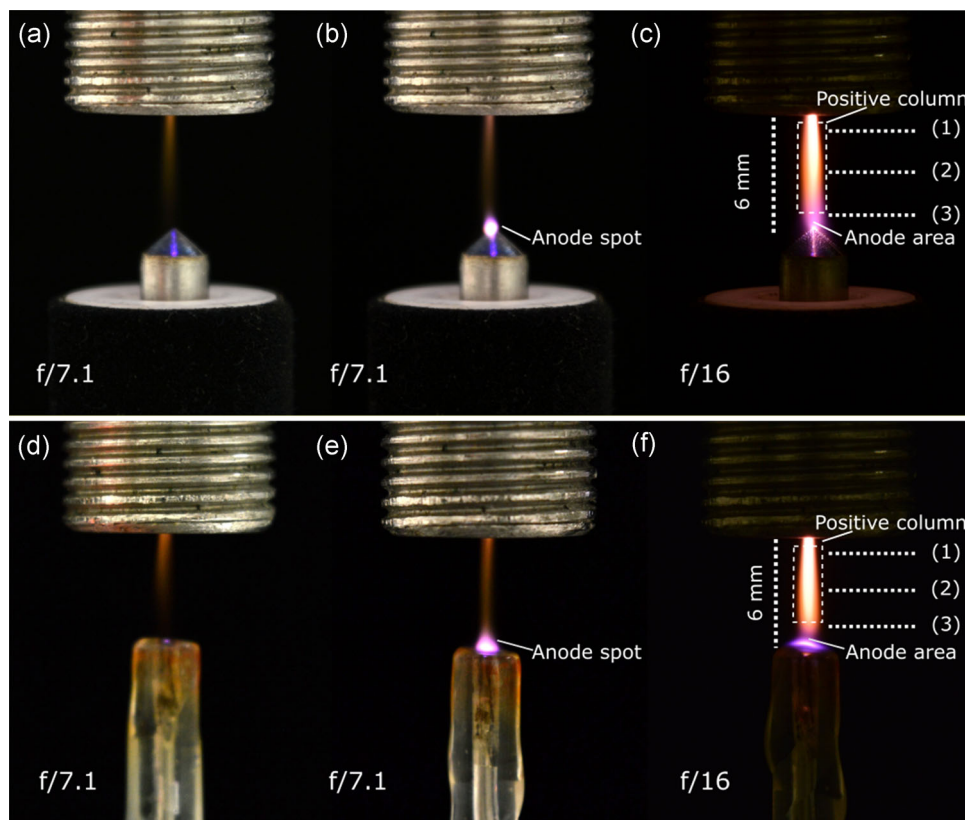


FIGURE 3 Images of the non-self-sustained discharge with indicating areas as a function of the anode applied voltage for the case of bottom metal electrodes (a–c) and bottom liquid electrode (d–f)

3 | RESULTS AND DISCUSSIONS

The phenomenology of the discharge ignition between the cathode and solid anode and between the cathode and liquid anode was firstly studied through measurements of the current–voltage characteristics and high-resolution images. On the basis of the voltage–current characteristics of the discharge, the value of the electrical field in the positive column of the glow was estimated. In the second section of the paper, the focus is on studying energy dissipation on vibrational, rotational, and translation stages of N_2 ground and excited states.

3.1 | Electrical characterization of NS-DG

The structure and visual view of the non-self-sustained discharge with an indication of the discharge areas depending on the applied anode voltage are presented in Figure 3. Images (a) and (d) are representing the case when only the plasma jet of the internal source is formed while the anode voltage of the main discharge is zero. Increasing the anode voltage results in the generation of a bright spot near the anode, Figure 3b,e, a predischage phase. This stage is characterized by a fast increase of the

current with the applied voltage, as indicated in Figure 4, left region with the current below 0.8 mA. In the predischage phase, the anode spot has been already formed by the amount of the electrons, which can reach the third electrode, and is still too low to form a complete breakdown of the main gap. Further increase of the applied voltage results in non-self-sustained discharge

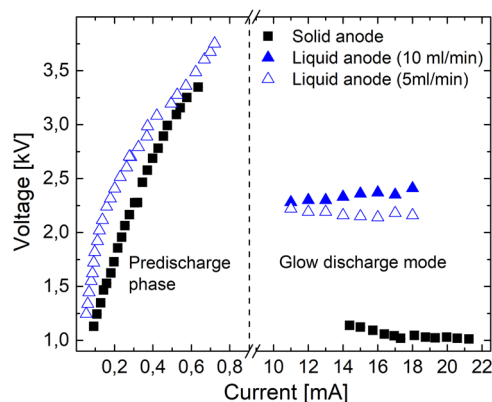


FIGURE 4 Current–voltage characteristic of the non-self-sustained discharge experimental conditions. Solid anode: The gas-flow through the jet and the third electrode are 2 and 1.5 SLM, respectively. Liquid anode: The jet gas-flow is 2 SLM, the water flow is 5 and 10 ml/min, respectively

formation with the generation of the “classical” structure of the glow discharge with a well-defined anode spot, dark space, and positive column (Figure 3c,f).^[2]

The dependence of the current passing through the anode with respect to the voltage in the main discharge gap is shown in Figure 4. The glow discharge is formed when the discharge current reaches a value of about 0.8 mA, Figure 4 region on the right. Interestingly, there is a significant difference in the voltage that required maintaining a non-sustained discharge with solid and liquid anode. The plasma with a solid anode can operate in a normal glow regime at the average voltage value of 1 kV. In the case of the liquid electrode, the average voltage value is twice higher of about 2.25 kV and a variation of the water flow rate allows switching the working regime from a normal glow at 5 ml/min to an abnormal glow at 10 ml/min. To reduce the residence time of the liquid in the contact with plasma and, thereby, reduce the variation of the conductivity during the discharge operation, the liquid flow of 10 ml/min has been chosen as a working condition for all experiments. During the predischage phase, the current and voltage of the internal ionization source stay stable (7 mA and 1 kV) and only a small current is passing through the main discharge gap as indicated in Figure 4. At the moment of transition from the predischage phase to the glow, the current passing through the main discharge increases and the overall current in both the main gap and internal sources becomes comparable. It should be noted that in the glow mode most of the current flows from the anode to the cathode and only a small current leakage (~10 μ A) to the ground is detected. This current behavior of the studied here sources is very similar to the micro hollow sustained glow discharge as indicated in Reference^[16].

It is interesting to define the operational mode of the discharge and ionization degree achieved in NS-GD. On the basis of current density, the electron density in the glow discharge positive column can be estimated by using the equation:

$$n_e = \frac{j}{E\mu_e e}, \quad (3)$$

where j is the current density, E is the electrical field calculated experimentally, and μ_e is electron mobility. The diameter of the positive column was determined as 2 mm based on the results of the Rayleigh scattering spectroscopy. Assuming an experimentally determined electrical field, the electron temperature and mobility can be estimated using a BOLSIG+ solver. The electrical field experimental data were obtained for the constant current of 17 mA, the same current was used for the current density determination.

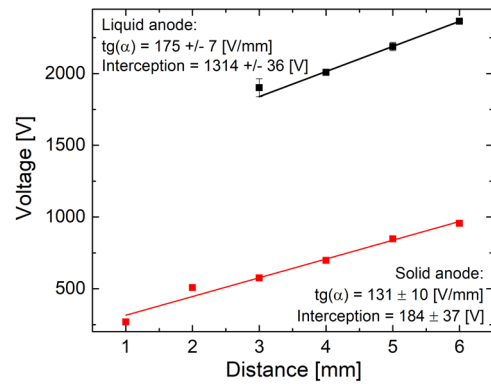


FIGURE 5 The electrical field and voltage drop on the electrode estimated based on the method of movable electrodes

The unknown value of the electrical field, E , is determined based on the measured applied voltage with a movable electrode at a constant discharge current as a slope of the plots presented in Figure 5. Plasma parameters for the solid and the liquid additional electrode systems, at the sustained current of 17 mA, are presented in Table 1. An experimentally obtained gas temperature, see Section 3.2, was used to estimate the reduced electrical field value E/n .

It has to be emphasized that the interception point in Figure 5 gives a value of the voltage drop on the anode. The large difference between voltage drop on the metal electrode of 184 V and liquid electrode of 1,314 V is explained by different processes of the anode spot formation and an additional voltage drop on the liquid layer. Obviously, in the case of the liquid electrode, the resistivity of the water column on top of the stainless steel needle submerged into the quartz capillary has to be taken into account, to estimate the anode voltage drop correctly. This can be made if the volume of the liquid in between the surface and submerged electrode is known. For instance, in our case, the calculated resistivity of the water column is 18 k Ω , which corresponds to the voltage drop of 310 V at the current of 17 mA. Thus, the real

TABLE 1 Main plasma parameters defined based on temperature measurements by Rayleigh scattering and estimations of the electrical field at the discharge current of 17 mA

Parameter	Solid anode	Liquid anode
Electrical field, E (V/cm)	1,308	1,750
Gas temperature, T_g (K)	1,571	1,453
Reduce electrical field, E/n (Td)	28	34
Current density, j (A/cm ²)	0.54	0.54
Electron mobility, μ_e (V cm ⁻¹ · s ⁻¹)	1.39×10^{22}	1.26×10^{22}
Electron density, n_e (cm ⁻³)	8.7×10^{11}	7.75×10^{11}
Electron temperature, T_e (K)	12,412	12,644

anode voltage drop on the liquid anode is 1 kV, which is still almost five times higher than the anode voltage drop for the metal electrode.

In the work published by Barinov et al.,^[26] the electrical field close to the anode of a self-sustained DC discharge between non-metallic-tap water electrodes was estimated to be $E \approx 2$ kV/cm and the average electron density n_e was in the range of 4×10^{11} – 7×10^{11} cm⁻³. Using their data, the reduced electrical field can be estimated in a few tens of Td, which agrees very well with our results for the discharge with the liquid electrode. Atmospheric pressure DC normal glow discharge in nitrogen between two metal electrodes was investigated by Staack et al.^[27] The electric field E was determined at 1,650 V/cm, which corresponds to the reduced electric field of 20 Td, at the gas temperature 887 K and the current of 3.5 mA. That is also in good agreement with our data for the solid anode. The discharge generated in this study is obviously similar to glow self-sustained as the value of the reduced electric field strength E in dielectric barrier discharges is typically about 150 Td^[28] and even can achieve a few thousand Td in the corona.^[29]

The reduced electrical field value corrected for gas density was estimated for all plasma currents, as shown in Figure 6. Experimentally measured gas temperature was used to estimate the Loschmidt number n .

The discharge in between metal/liquid electrodes can be sustained at a lower E/n value below 20 Td at the current range of 10–13 mA. However, the E/n value required to sustain the discharge increases much faster with an increase of the current in the case of the liquid anode. Higher E/n in the discharge with the liquid electrode can be explained by the difference in plasma conductivity compared to the metal electrodes and the difference in processes near the liquid anode playing the role of resistive barrier similar to mechanisms described in Reference^[30]. It has to be noted that the effect of H₂O

admiring in the positive column of the discharge due to electrode evaporation and sputtering has been neglected in Equation (3) and Table 1 because of high N₂ flow directed towards the anode. However, water evaporation is an important process in plasma formation near the anode as will be shown in Sections 3.2 and 3.3.

3.2 | Vibrational, rotational, and translation temperature

Atmospheric pressure plasma operation in strongly non-equilibrium conditions is highly beneficial for the initiation of many chemical processes in the gas and liquid phase, including CO₂ reforming, N₂ fixation, water treatment, and others.^[4,5,31–34] In this regard, special attention is given to determine the gas temperature to get insights into the mechanisms and kinetics of N₂ excitation in NS-GD. Optical emission spectroscopy was used to obtain rotational and vibrational temperatures of N₂ excited state molecules, whereas Rayleigh scattering spectroscopy was used to measure the translational temperature of N₂ ground-state molecules. An overview of the spectrum in the range of 250–900 nm of a positive column is presented in Figure 7a for both solid and liquid anode for the current of 17 mA. Space-resolved spectrum for three positions, which will be referred to as 1—cathode, 2—positive column, 3—anode, indicated in Figure 3f in the case of the liquid anode is given in Figure 7b.

Four vibrational peaks of a second positive system of nitrogen N₂ C³Π_u→B³Π_g ($\Delta v = 0-2, 1-3, 2-4, \text{ and } 3-5$) were fitted with the use of MassiveOES^[22,23] to obtain both T_{vib} and T_{rot} of N₂ excited states. An example of the fitting result for a case of the metal additional electrode at the discharge current of 12 mA is presented in Figure 8. Space-resolved vibrational and rotational temperature for different discharge current for both discharge configurations (with metal and liquid anode) are presented in Figure 8a,b.

The current increasing leads to gas heating and, thus, increasing of T_{rot} is observed for both discharges with the solid and liquid electrode (Figure 9). It is found that the rotational temperature for the solid anode is in the range of 2,000–2,700 K near the anode and slightly higher at 2,400–3,000 K in the positive column and the cathode area. Replacement of the metal electrode by liquid results in a lower T_{rot} near the anode of about 1,900–2,400 K, depending on the current. The observed effect of the liquid electrode can be attributed to energy transfer from N₂ excited states to OH radicals appearing because of water evaporation in the anode region, as indicated by the following reaction:

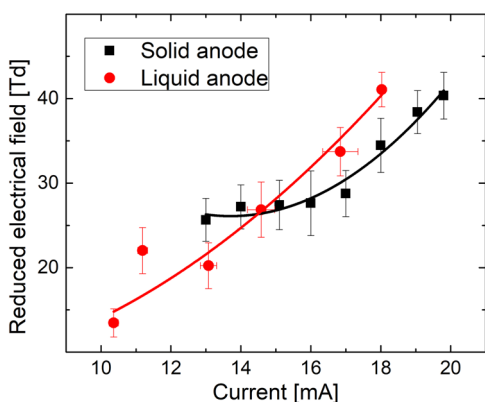
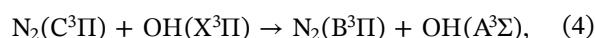


FIGURE 6 The reduced electrical field E/n as a function of the discharge current for metal/metal and metal/liquid electrodes

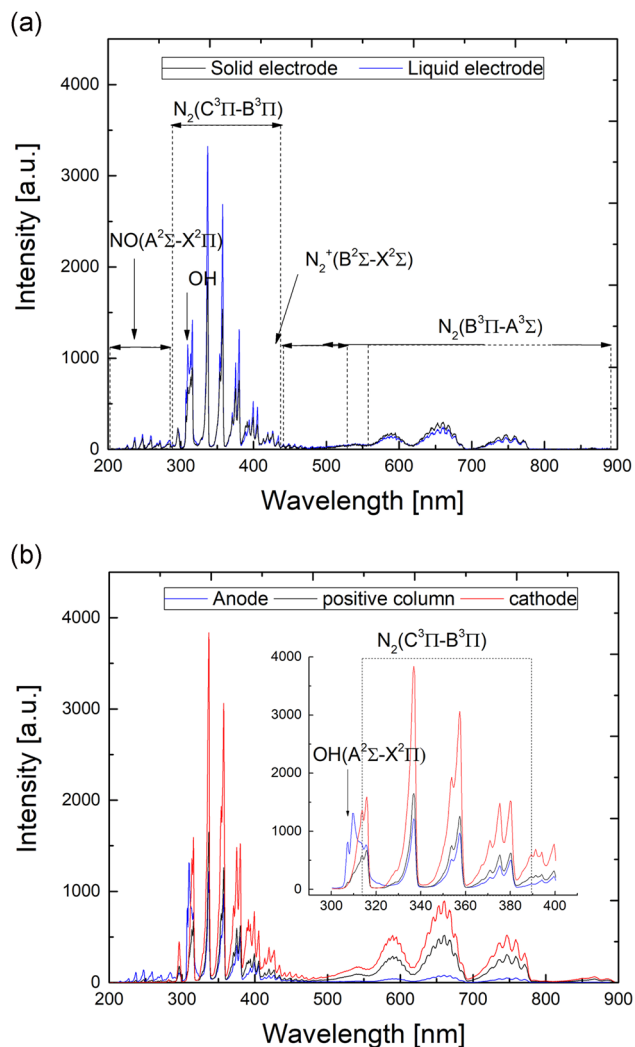


FIGURE 7 Overview of nitrogen NS-DG spectrum in the range of 200–900 nm for current 17 mA (a) in the region of the positive column for metal/metal and metal/liquid anode. (b) Space-resolved spectrum for three positions in the case of metal/liquid anode

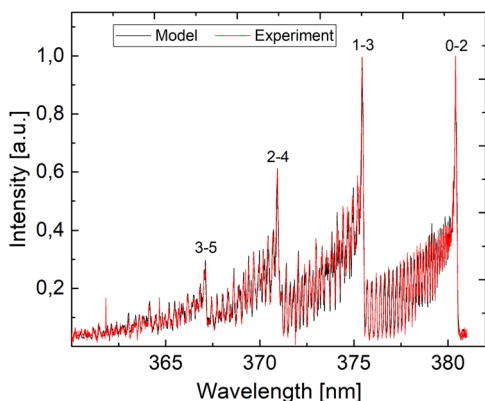


FIGURE 8 Example of MassiveOES simulation of the discharge spectrum obtained in the metal/metal electrode systems at the current of 12 mA. Best fitting has been obtained with $T_{\text{vib}} = 6,302 \pm 69$ K and $T_{\text{rot}} = 2,068 \pm 20$ K (fitting error)

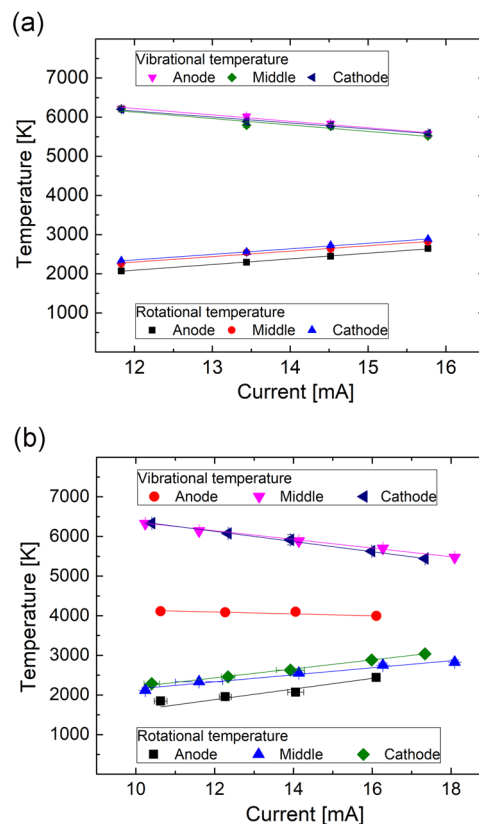
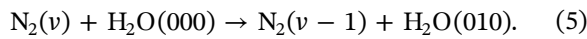


FIGURE 9 Vibrational and rotational temperature measurement in three positions corresponding to the anode, positive column, and cathode region by means of emission spectroscopy: (a) metal/metal electrodes; (b) metal/liquid electrodes

where the difference between energy levels for transitions are $\Delta E_{\text{OH}(X-A)} = 4.01$ eV and $\Delta E_{\text{N}_2(C-B)} = 3.68$ eV. This process well agrees with a decrease of intensity of N₂(C³Π_u-B³Π_g) band observed near the anode, see inset in Figure 7b.

It is important to note that NS-GD is operating in highly non-equilibrium conditions as indicated by the measured vibrational and electron temperature for both solid and liquid anode proving the validity of condition $T_e > T_{\text{vib}} > T_{\text{rot}} \geq T_{\text{gas}}$. In both discharges, the highest T_{vib} of 6,500 K is observed at the lowest discharge current in the positive column and near the cathode. In opposition to T_{rot} , the increase of the discharge current results in a fast almost linear drop in T_{vib} with the increase of the current. It is known that the rate of vibrational–translational energy transfer k_{V-T} exponentially increases with translational temperature $k_{V-T} \approx \exp(T^{-1/3})$.^[35] Accordingly, a decrease of vibrational temperature with gas heating can be related to effective vibrational–translational transfer at higher gas temperatures (at $T_g \sim 1,000$ K, $k_{V-T} = 10^{-15}$ cm³/s) compared to room temperature ($T \sim 300$ K, $k_{V-T} = 10^{-21}$ cm³/s).^[36] An increase of V–T transfer efficiency at

high gas temperature (and so T_{rot}) is responsible for the discharge thermalization and clearly visible in experiments, see Figure 9a,b. Very similar T_{vib} and T_e in the positive column of discharges with different electrodes confirm the negligible effect of water evaporation on the plasma properties at a long distance from the liquid. However, much lower T_{vib} in the range of 4,100–3,900 K was measured near the liquid anode. Near the liquid, evaporation of H_2O cannot be neglected anymore and starts to be important. Indeed, it was reported that quenching of vibrationally excited N_2 with water molecules plays an important role at higher temperatures ($T \sim 1,000$ K, $k_{\text{V-V}} = 10^{-13} \text{ cm}^3/\text{s}$),^[37] thus the 2,000 K lower vibrational temperature of N_2 near the liquid anode area is partially explained by the following process:



Consequently, the mechanisms (4) and (5) can influence the excitation of N_2 states and leads to a lower vibrational temperature near the liquid anode.

At high pressure, the rotational temperature is well representative of the gas (translational) temperature due to the high frequency of collisions leading to very fast rotational/translation (RT) equilibrium in the system. However, in a number of cases, even at high pressure, the rotational temperature was found to be different from the translational one.^[21,38,39] It was found that excitation processes realized in the discharge results in overpopulation of specific rotational states and so can lead to overestimation of the gas temperature obtained by emission spectroscopy. Rayleigh scattering spectroscopy was used in the present study to determine the translational gas temperature in plasma as described in Section 2. Results presented on Figure 10a correspond to the temperature in the discharge core, while the example of temperature profiles, for both electrodes, is shown in Figure 10b. It should be noted that images of interest were free of Mie scattering, so the uncertainty of results is defined by the laser energy fluctuation, which is measured to be 10%.

Gas temperature, when the solid electrode was used, is found to be in a range of 1,200–2,400 K for currents of 13–20 mA, whereas a lower gas temperature is measured in plasma with the liquid anode and is about 650–1,700 K for the operational current range 10–16 mA. The slightly lower gas temperature in the case of the liquid anode is probably due to the cooling effect of gas above the liquid due to water evaporation similar to the observed effect for T_{rot} in Figure 8. The difference in rotational temperature obtained by OES and translational temperature obtained by Rayleigh spectroscopy is explained by the deviation of the discharge from RT equilibrium.^[21] The discrepancy between the translational and rotational temperatures

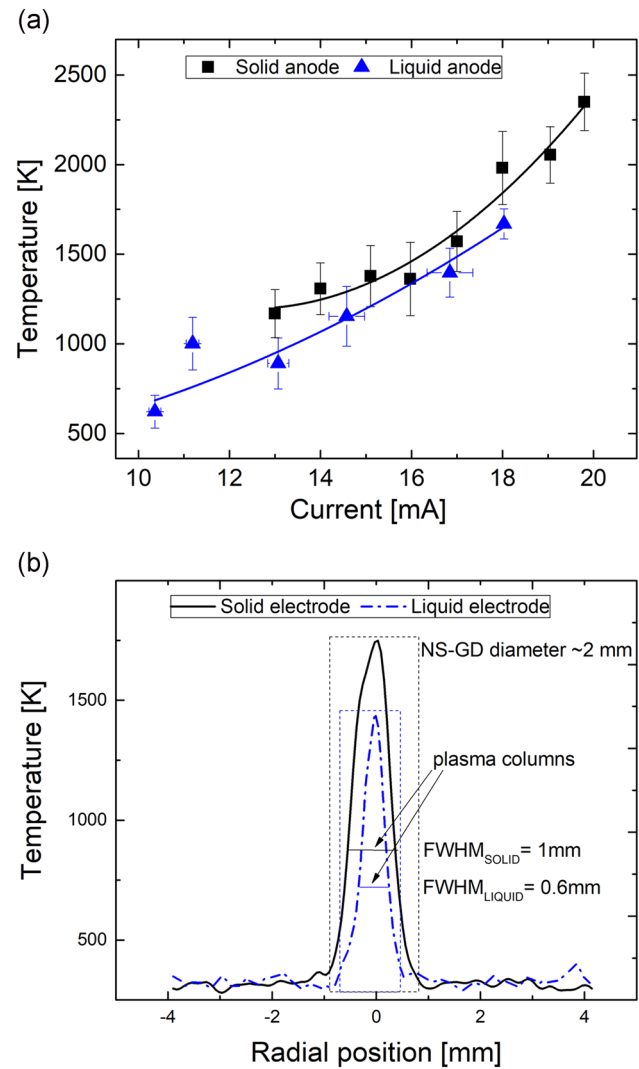
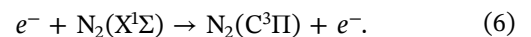


FIGURE 10 Results of the Rayleigh scattering spectroscopy. (a) Gas temperature in the core of the plasma column versus discharge current for the solid and liquid anodes. (b) Gas temperature profile for discharge current of 18 mA

might be due to the fact that T_{gas} is not high enough to provide effective and fast rotational energy transfer and so complete thermalization of translational and rotational degrees of freedom. Additionally, the $\text{N}_2(\text{C}^3\Pi)$ state might not be populated only by direct electron excitation through the following reaction:



Indeed, the large difference between T_g and T_{rot} , especially at low currents, is indicative of the complex excitation mechanism of $\text{N}_2(\text{C}^3\Pi)$. A similar behavior was reported for gliding arc discharge with temperatures $T_{\text{rot}} = 4,300 \pm 400$ K and $T_{\text{gas}} = 1,100 \pm 260$ K determined using the same experimental techniques^[39] and also in hybrid gliding arc (air + water vapor) discharge.^[40]

As shown in Reference^[21] in non-equilibrium plasmas, the Boltzmann population of the rotational states cannot be described by only one rotational temperature. An example of the population distribution for different rotational levels of J_4 - J_{30} , for NS-GD, is shown in Figure 11. Obviously, different slopes with temperatures T_1 , T_2 , and T_3 can be distinguished and correspond to different excitation mechanisms of the $N_2(C^3\Pi_u)$ state. Table 2 presents the T_{rot} obtained considering different J ranges for liquid and solid electrodes at the anode region. A good agreement with Rayleigh scattering temperature measurements can be seen for J numbers in the range of J_{12} - J_{20} . In the case of the solid anode, T_2 is comparable with T_{gas} and has the same tendency with the increase of the current. In the case of the liquid anode, there is a difference between T_g and T_2 at the lowest current, which can be explained by temporal instability of the discharge, which starts to be negligible at a higher current, where results of Rayleigh scattering and emission spectroscopy perfectly match each other.

3.3 | Excitation mechanisms of N_2 states

Optical emission spectroscopy can be implemented for electrical field strength determination in air or nitrogen plasmas at atmospheric pressure.^[41-47] The excitation energy of the $N_2(C^3\Pi_u, v=0)$ and $N_2^+(B^2\Sigma_u^+, v=0)$, which belong to the SPS of $N_2(C^3\Pi_u \rightarrow B^3\Pi_g)$ and the first negative system (FNS) of $N_2^+(B^2\Sigma_u^+ \rightarrow X^2\Sigma_g^+)$, are 11.03 and 18.7 eV, respectively. This significant energy difference makes their intensity ratio quite sensitive to electron energy and, consequently, to the reduced electrical field. In the approximation that the excitation mechanism of the $N_2(C^3\Pi_u)$ and $N_2^+(B^2\Sigma_u^+)$ has taken place only by

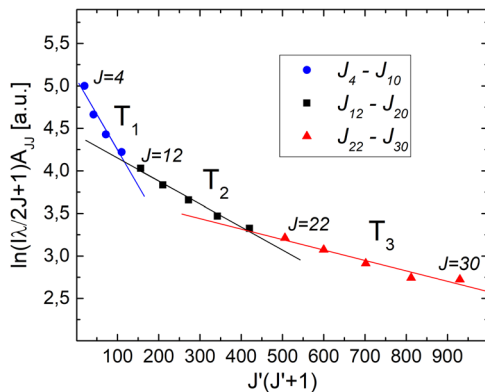
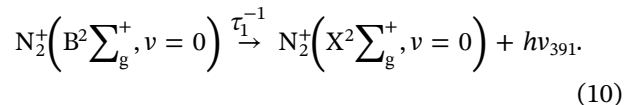
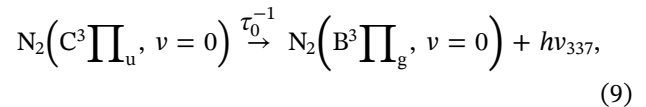
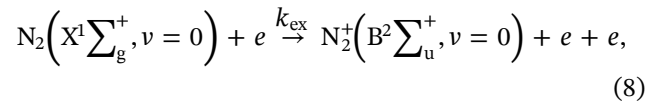
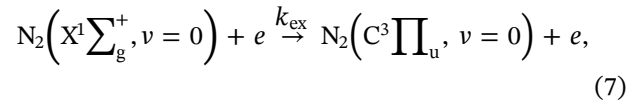


FIGURE 11 An example of the non-equilibrium rotational distribution of $N_2(C^3\Pi_u)$ for discharge with the liquid anode, in the anode position of the fiber, at the current of 10.5 mA. Boltzmann plot fitting was performed with correlation not lower than 0.99 in the specified ranges of J numbers

TABLE 2 Comparison of gas temperature and Boltzmann plot method with a variable range of J numbers

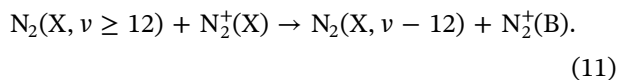
Current, I (mA)	Rotational temperatures with respect to J levels, T_{rot} (K)		Gas temperature (K)
	T_2 (J_{12} - J_{20})	T_3 (J_{22} - J_{30})	
<i>Solid additional electrode (anode position)</i>			
12	1,239 ± 102	3,039 ± 387	1,169 ± 134 (13 mA)
13.5	1,399 ± 85	3,086 ± 235	1,307 ± 144 (14 mA)
14.5	1,422 ± 100	3,339 ± 354	1,378 ± 170 (15 mA)
16	1,545 ± 104	3,662 ± 161	1,362 ± 205
<i>Liquid additional electrode (anode position)</i>			
10.5	1,049 ± 75	2,386 ± 328	622 ± 91
12.5	1,168 ± 90	2,778 ± 229	891 ± 142
14	1,246 ± 78	2,810 ± 231	1,154 ± 167
16	1,374 ± 114	3,291 ± 339	1,397 ± 137

direct electron impact, we can write the following scheme of the excitation/ionization processes:



Corresponding to the considered reactions (7)–(10), the reduced electrical field can be estimated from a ratio of line intensity at 337 and 391 nm. Indeed, Paris et al.^[41] have applied this method in a wide pressure range, from 300 to 10^5 Pa, for air discharge. The approach of Paris et al., which is based on electron-impact excitation was applied to estimate the E-field in NS-GD. to record vibrational transitions $N_2(C^3\Pi_u)$ and $N_2^+(B^2\Sigma_u^+)$ simultaneously, an Ocean Optics spectrometer with wide range detection was used. The fiber was set in the same positions as for the temperature determination by OES (see Section 2.3.1). Experimentally measured gas temperature (Figure 9a) was used to estimate the Loschmidt

number n_0 . Radiative lifetime τ_0 , τ_1 , and deactivation rate constants k_q due to quenching of N_2 radiative states were taken to be the same as in Paris et al.^[41] Interestingly, the reduced electrical field value E/n_0 , at the lowest current, was found to be several hundreds of Td and decreases with the increase of the current. In the positive column, at the discharge current of 17 mA, the E/n determined by spectroscopic method assuming the direct electron excitation mechanism was 640 and 570 Td for the solid and the liquid anode, respectively. These results are contradictory to experimental values (see Section 3.1) for the solid and liquid anode, where E/n values were found at 28 and 34 Td, at the same sustained current of 17 mA. Measured E/n values as a function of the discharge current have shown (see Figure 6) that even at the highest currents the E/n does not exceed 50 Td for both solid and liquid electrodes. This strong discrepancy, between the model and the experiments, means the set of reactions (7)–(10), assuming only direct electron excitation, is not sufficient at describing the nitrogen excitation in NS-GD. As was shown in Reference^[1], at a reduced electrical field below 100 Td, the most dominant excitation mechanism of the nitrogen states is vibrational excitation. Capitelli et al.^[48] also found that the main excitation channel of the N_2 and formation of FNS, the transition N_2^+ ($B^2\Sigma_u^+ \rightarrow X^2\Sigma_g^+$), is:



This mechanism through vibrational state excitation leads to a higher density population of the N_2^+ ($B^2\Sigma_u^+$) states regarding direct electron-impact ionization that, consequently, increases the intensity of the line N_2^+ ($B^2\Sigma_u^+ \rightarrow X^2\Sigma_g^+$) at 391 nm. Accordingly, a strong increase of the line ratio I_{391}/I_{337} that results in the overestimation of the reduced E-field in NS-GD based on the mechanism (7)–(10) is detected. This is in good agreement with the aforementioned results and indicates effective vibrational excitation of N_2 states in a NS-GD.

4 | CONCLUSIONS

DC NS-GD, operating at atmospheric pressure, was studied as a source of non-thermal plasma. An N_2 jet was used as an internal source of ionization, and NS-GD with metal and liquid additional electrodes was generated at low operational voltage. For a better understanding of nitrogen molecule excitation mechanisms, a set of electrical and temperature diagnostic techniques was applied. It was found that the low-current predischARGE

phase appears before the breakdown. Above 1 kV for solid and 2.2 kV for liquid electrode, in the current range of 10–20 mA, the discharge operates in glow regime as a diffuse plasma with 2-mm diameter and 6-mm length. The current density was used to estimate electron density, which is in the range $n_e \approx 6\text{--}9 \times 10^{11} \text{ cm}^{-3}$. Optical emission spectroscopy and Rayleigh scattering were applied for temperature characterization of the discharge. Non-equilibrium behavior of the discharge was noticed as vibrational $T_{\text{vib}} \approx 6,000 \text{ K}$ of N_2 excited states was almost three times higher than rotational $T_{\text{rot}} > 2,000 \text{ K}$ N_2 temperature. With the increase of the current, heating of the gas and V–T transfer starts to be significant and the discharge approaches thermal equilibrium. The translational gas temperature obtained by Rayleigh scattering was considerably lower than the rotational temperature of the N_2 excited states and was in the range of $T_g \approx 1,170\text{--}2,000 \text{ K}$ for solid and $T_g \approx 900\text{--}1,670 \text{ K}$ for the liquid anode in the current range of 13–18 mA. The higher N_2 rotational temperature compared to translational temperature indicates the importance of N_2 excitation processes different from direct electron excitation. The vibrational excitation of N_2 states has been validated by comparing the reduced electrical field measured experimentally with a value estimated via the intensity ratio of nitrogen lines N_2 (337 nm)/ N_2^+ (391 nm), which is based solely on N_2 direct electron excitation. It was found that the ionization of N_2 by means of the vibrational pathway is an important process in NS-GD because of the relatively low reduced electrical field in the positive column supporting vibrational excitation processes.

ACKNOWLEDGMENTS

The authors acknowledge the NITROPLASM EOS project (ID: 30505023) and thank the support of the work by FWO/ARRS agencies, project numbers G084917N and N3-0056.

ORCID

Mikhail Gromov  <http://orcid.org/0000-0002-6543-8914>

REFERENCES

- [1] A. Fridman, L. A. Kennedy, *Plasma Physics and Engineering*, CRC Press, New York **2004**.
- [2] M. A. Lieberman, A. J. Lichtenberg, *Principles of Plasma Discharges and Materials Processing*, John Wiley & Sons, Hoboken, New Jersey **2005**.
- [3] G. Fridman, G. Friedman, A. Gutsol, A. B. Shekhter, V. N. Vasilets, A. Fridman, *Plasma Process. Polym.* **2008**, 5, 503.

- [4] A. Bogaerts, E. C. Neyts, *ACS Energy Lett.* **2018**, 3, 1013.
- [5] A. Anastasopoulou, Q. Wang, V. Hessel, J. Lang, *Processes* **2014**, 2, 694.
- [6] N. Cherkasov, A. O. Ibhadon, P. Fitzpatrick, *Chem. Eng. Process. Process Intensif.* **2015**, 90, 24.
- [7] W. Wang, B. Patil, S. Heijkers, V. Hessel, A. Bogaerts, *ChemSusChem* **2017**, 10, 2110.
- [8] P. J. Bruggeman, F. Iza, R. Brandenburg, *Plasma Sources Sci. Technol.* **2017**, 26.
- [9] A. P. Napartovich, *Plasmas Polym* **2001**, 6, 1.
- [10] Y. Akishev, M. Grushin, I. Kochetov, V. Karal'Nik, A. Napartovich, N. Trushkin, *Plasma Sources Sci. Technol.* **2005**, 14.
- [11] Y. Raizer. *Gas Discharge Physics*, Springer, Berlin **1991**.
- [12] Y. Akishev, O. Goossens, T. Callebaut, C. Leys, A. Napartovich, N. Trushkin, *J. Phys. D: Appl. Phys.* **2001**, 34, 2875.
- [13] R. H. Stark, K. H. Schoenbach, *J. Appl. Phys.* **1999**, 85, 2075.
- [14] F. Leipold, R. H. Stark, A. El-Habachi, K. H. Schoenbach, *J. Phys. D: Appl. Phys.* **2000**, 33, 2268.
- [15] R. H. Stark, K. H. Schoenbach, *J. Appl. Phys.* **2001**, 89, 3568.
- [16] A. A. H. Mohamed, R. Block, K. H. Schoenbach, *IEEE Trans. Plasma Sci.* **2002**, 30, 182.
- [17] K. H. Schoenbach, R. Verhappen, T. Tessnow, F. E. Peterkin, W. W. Byszewski, *Appl. Phys. Lett.* **1995**, 13, 13.
- [18] K. H. Schoenbach, A. El-Habachi, M. M. Moselhy, W. Shi, R. H. Stark, *Phys. Plasmas* **2000**, 7, 2186.
- [19] W. Shi, R. H. Stark, K. H. Schoenbach, *IEEE Trans. Plasma Sci.* **1999**, 27, 16.
- [20] S. Li, J. Medrano Jimenez, V. Hessel, F. Gallucci, *Processes* **2018**, 6, 248.
- [21] P. J. Bruggeman, N. Sadeghi, D. C. Schram, V. Linss, *Plasma Sources Sci. Technol.* **2014**, 23, 23001.
- [22] J. Voráč, P. Synek, V. Procházka, T. Hoder, *J. Phys. D: Appl. Phys.* **2017**, 50.
- [23] J. Voráč, P. Synek, L. Potočnáková, J. Hnilica, V. Kudrle, *Plasma Sources Sci. Technol.* **2017**, 26.
- [24] R. B. Miles, W. R. Lempert, J. N. Forkey, *Meas. Sci. Technol.* **2001**, 12, R33.
- [25] M. Sneep, W. Ubachs, *J. Quant. Spectrosc. Radiat. Transf.* **2005**, 92, 293.
- [26] Y. A. Barinov, V. B. Kaplan, V. V. Rozhdestvenskii, S. M. Shkol'nik, *Tech. Phys. Lett.* **1998**, 24, 929.
- [27] D. Staack, B. Farouk, A. Gutsol, A. Fridman, *Plasma Sources Sci. Technol.* **2008**, 17.
- [28] H. E. Wagner, R. Brandenburg, K. V. Kozlov, A. Sonnenfeld, P. Michel, J. F. Behnke, *User Model. User-Adapt. Interact.* **2003**, 71, 417.
- [29] J. S. Chang, P. A. Lawless, T. Yamamoto, *IEEE Trans. Plasma Sci.* **1991**, 19, 1152.
- [30] T. Verreycken, D. C. Schram, C. Leys, P. Bruggeman, *Plasma Sources Sci. Technol.* **2010**, 19.
- [31] T. Silva, N. Britun, T. Godfroid, R. Snyders, *Plasma Sci. Technol. Prog. Phys. States Chem. React.* **2016**, 479.
- [32] A. Fridman, Y. Yang, Y. I. Cho, *Plasma Discharge in Liquid: Water Treatment and Applications*, CRC Press, California **2012**.
- [33] V. V. Rybkin, D. A. Shutov, *Plasma Phys. Rep.* **2017**, 43, 1089.
- [34] B. Jiang, J. Zheng, S. Qiu, M. Wu, Q. Zhang, Z. Yan, Q. Xue, *Chem. Eng. J.* **2014**, 236, 348.
- [35] A. Lifshitz, *J. Chem. Phys.* **1974**, 61, 2478.
- [36] M. Cacciatore, A. Kurnosov, A. Napartovich, *J. Chem. Phys.* **2005**, 123, 174315.
- [37] R. J. McNeal, M. E. Whitson Jr, G. R. Cook, *J. Geophys. Res.* **1974**, 79, 1527.
- [38] T. Verreycken, A. F. H. van Gessel, A. Pageau, P. Bruggeman, *Plasma Sources Sci. Technol.* **2011**, 20.
- [39] J. Zhu, A. Ehn, J. Gao, C. Kong, M. Aldén, M. Salewski, F. Leipold, Y. Kusano, Z. Li, *Opt. Express* **2017**, 25, 20243.
- [40] X. Tu, L. Yu, J. H. Yan, K. F. Cen, B. G. Chéron, *Phys. Plasmas* **2009**, 16, 113506.
- [41] P. Paris, M. Aints, F. Valk, T. Plank, A. Haljaste, K. V. Kozlov, H. E. Wagner, *J. Phys. D: Appl. Phys.* **2005**, 38, 3894.
- [42] S. Pancheshnyi, *J. Phys. D: Appl. Phys.* **2006**, 39, 1708.
- [43] P. Paris, M. Aints, F. Valk, T. Plank, A. Haljaste, K. V. Kozlov, H. E. Wagner, *J. Phys. D: Appl. Phys.* **2006**, 39, 2636.
- [44] P. Paris, M. Aints, M. Laan, F. Valk, *J. Phys. D: Appl. Phys.* **2004**, 37, 1179.
- [45] K. V. Kozlov, H. E. Wagner, R. Brandenburg, P. Michel, *J. Phys. D: Appl. Phys.* **2001**, 34, 3164.
- [46] T. Hoder, M. Sira, H.-E. Kozlov, *J. Phys. D* **2008**, 41, 035212.
- [47] G. Dilecce, P. F. Ambrico, S. De Benedictis, *J. Phys. D: Appl. Phys.* **2010**, 43.
- [48] M. Capitelli, C. M. Ferreira, B. F. Gordiets, A. I. Osipov, *Plasma Kinetics in Atmospheric Gases*, Springer Science & Business Media, Berlin **2013**, 31.

How to cite this article: Sremački I, Gromov M, Leys C, Morent R, Snyders R, Nikiforov A. An atmospheric pressure non-self-sustained glow discharge in between metal/metal and metal/liquid electrodes. *Plasma Process Polym.* 2019;e1900191. <https://doi.org/10.1002/ppap.201900191>